LICENTIATE THESIS

Experiments and simulations on the mechanics of ice and snow

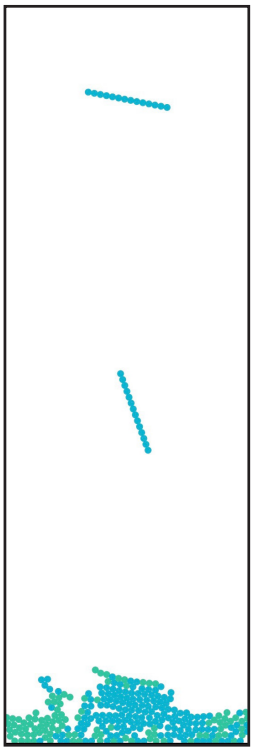

Hassan Bahaloohoreh

Mechanics of ice and snow

LULEÅ UNIVERSITY OF TECHNOLOGY

Thesis for the degree: Teknologie Licentiate
Thesis advisors: Johan Casselgren, Mikael Sjödahl, and Fredrik Forsberg

Cover Figure: Computer simulation of model snow filling in a container

Acknowledgements

I would like to start by thanking my supervisors Mikael Sjödahl, Johan Casselgren, and Fredrik Frosberg. Mikael provided most insightful comments during the review of the manuscripts and was supportive during my PhD studies at LTU. Johan apart from being a good supervisor is a dexterous project leader with multitude of connections in industry; so, not surprisingly, he coordinated easily with parties outside LTU either for the purpose of experiments or some more industrial collaborations and networking. Fredrik was extremely helpful and supportive in conducting micro tomography scanning and post processing of data.

I would like to go on by appreciating the tremendous amount of help, support, and leanrings I received from Per Gren (as he says: one should never work with ice and snow since they are too complicated) during the experiments on ice. He is a unique person in the field of experimental mechanics and I wish I had the opportunity to learn more experimental techniques from him. When I talk about the experiments and micro tomography scanning, it is impossible to miss Henrik Lycksom, another unique person, who assisted me during the experiments either complicated scanning tasks or simpler tasks like providing required tools for some experiments. With his busy schedule, I never found him tired, or impatient.

For these wonderful people in the group with the capabilities and expertise spanning extensive area, the support I received as a PhD student within the experimental mechanics division was excellent. This is a reason that it feels so difficult to leave this group.

The discussions I has with Tobias Eidevåg, who was doing his industrial PhD research at Chalmers university of technology was really helpful and the help he provided to acquire an experimental device initially developed by Per Abrahamsson at Chalmers is invaluable. I would like to thank both of them.

I would also like to thank all the colleagues and friends in the division of the fluid and experimental mechanics which contributed for having such a nice research environment at LTU.

Last but not least, I would like to thank my friend and dear wife Atena Mohseni, for her supports and devotion during my "Irregular research life-style". It was impossible to smoothly progress in this research without her understanding.

Abstract

In this study, experiments and simulations were conducted to investigate ice and snow. The ice sintering force as a function of temperature, pressing force (contact load), contact duration, and particle size during the primary stage of sintering was formulated using experimental methods along with an approximate, semi-analytic, close-form solution. It was shown that the ice sintering force increases nearly linear with increasing external pressing force but best approximated as a power law for dependency on both contact duration and particle size. Moreover, the exponent of the power law for size dependence is around the value predicted by general sintering theory. The temperature dependence of the sintering force is highly nonlinear and follows the Arrhenius equation. It was observed that at temperatures closer to the melting point, a liquid bridge is observed upon the separation of the contacted ice particles. The ratio of ultimate tensile strength of ice to the axial stress concentration factor in tension is found as an important factor in determining the sintering force, and a value of nearly 1.1 MPa was estimated to best catch the sintering force of ice in different conditions. From the temperature dependency, the activation energy is calculated to be around 41.4 kJ/mol, which is close to the previously reported value. Also, the results for the sintering force suggest that smaller particles are "stickier" than larger particles. Moreover, cavitation and surface cracking is observed during the formation of the ice particles and these can be one of the sources for the variations observed in the measured ice sintering force values.

The presence of a capillary bridge in contact between an ice particle and a "smooth" (or rough) Aluminum surface at relative humidity around 50% and temperatures below the melting point was experimentally demonstrated. Experiments were conducted under controlled temperature conditions and the mechanical instability of the bridge upon separation of the ice particle from the Aluminum surface with a constant speed was considered. It was observed that a liquid bridge with a more pronounced volume at temperatures near the melting point is formed. It was showen that the separation distance is proportional to the cube root of the volume of the bridge. The volume of the liquid bridge is used to estimate the thickness of the liquid layer on the ice particle and the estimated value was shown to be within the range reported in the literature. The thickness of the liquid layer decreases from nearly 56 nm at -1.7°C to 0.2 nm at -12.7°C. The dependence can be approximated with a power law, proportional to $(T_M - T)^{-\beta}$, where $\beta < 2.6$. We further observe that for a rough surface, the capillary bridge formation in the considered experimental conditions vanishes.

The Discrete Element Method (DEM) was employed to simulate the filling behavior of dry snow. Snow as a heterogeneous, hot material which is constituted from spherical ice particles which can form bonds. The bonding behavior of ice particles is important in determining the macroscopic behavior of snow. The bond diameter of ice-ice contacts as a function of time, compressive load, and strain rate is used and a DEM for dry snow was developed and programmed in MATLAB. A beam element with implemented damage model was used in the simulation. The simulated parameters were macroscopic angle of repose, packing density, and surface conditions as a function of temperature and filling rate. The DEM results were able to verify the existing published experimental data. The simulation results showed that angle of repose of snow decreased with decreasing the temperature, the surface became irregular due to particles rotation and re-arrangement for lower falling speeds of particles, and density increased with depth of deposition.

Keywords: mechanics, ice, snow, sintering force, thin liquid layer, discrete element method

List of publications

Papers

Paper A : **Ice sintering: Dependence of sintering force on temperature, load, duration, and particle size**,
Hassan Bahaloo, Tobias Eidevåg, Per Gren, Johan Casselgren, Fredrik Forsberg, Per Abrahamsson, and Mikael Sjödahl,
J. Appl. Phys. 131, 025109 (2022)
doi:10.1063/5.0073824

Paper B : **Capillary bridge in contact of ice particles reveals the thin liquid film on ice**,
Hassan Bahaloo, Per Gren, Johan Casselgren, Fredrik Forsberg, and Mikael Sjödahl,
Submitted

Paper C : **Discrete element simulation of dry snow using the developed analytic bond model**,
Hassan Bahaloo, Johan Casselgren, Fredrik Forsberg, Mikael Sjödahl,
IOP Conf. Series: Materials Science and Engineering (2021)
doi:10.1088/1757-899X/1190/1/012015

Contents

I Summary

1 Introduction **1**
- 1.1 Motivation . . . 1
- 1.2 Literature review . . . 2
- 1.3 Thesis layout . . . 6

2 Methods **7**
- 2.1 Ice sintering force . . . 7
- 2.2 Liquid layer on the ice . . . 8
- 2.3 DEM programming . . . 11

3 Results **17**
- 3.1 Sintering force of ice . . . 17
- 3.2 Liquid layer on the ice . . . 20
- 3.3 DEM simulation . . . 21

4 Summary & Future work **25**
- 4.1 Summery . . . 25
- 4.2 Future work . . . 26

II Papers **37**

A Ice sintering: Dependence of sintering force on temperature, load, duration, and particle size **39**

B Capillary bridge in contact of ice particles reveals the thin liquid film on ice **53**

C Discrete element simulation of dry snow using the developed analytic bond model **69**

Part I

Summary

1 Introduction

1.1 Motivation

Ice and snow can cause huge burdens and associated costs to the societies. For example, the estimated cost between October 2014 and March 2015 in 23 states in the US to plow and treat roadways to keep traffic flowing was $1.13 billion [1]. Considering that the plowing machines are almost always overloaded due to the lack of detailed knowledge about snow shear strength to ensure a sustained snow removal, any decrements in the machine load which may result in a change of machine type (as well), has the potential to hugely reduce the costs. Despite this, our understanding of ice and snow mechanical properties are not complete.

Part of the problem is that the behavior of ice and snow is complex with a pronounced viscous behavior. The difficulty can be exacerbated with the volume change during the volumetric loading which makes the material a visco-plastic one. More challenging, ice and snow are materials which exist almost always near their melting points.

Creep and relaxation are two main characteristics of visco-elastic materials. Creep of a material can be described as a gradual increase in the strain under the application of a constant load or stress. Relaxation is the decay in stress response under a constant displacement.

Ice particles stick together immediately when they are brought into contact either under gentle or sever loading REF. There used to be different explanations for this phenomenon but nowadays it is widely accepted that there is a liquid or ***quasi-liquid layer (QLL)*** on the ice particle for temperatures well below the melting point and this QLL is responsible

for this quick sticking.

In this study, we try to shed some light on the micro mechanics of ice and conduct simulations on snow behavior. The micro mechanics of ice gives rise to the macro mechanics of snow. We put forward the questions:

1. How do the sintering force between ice particles depend on size, temperature, time, and external pressing load?
2. What would be the sticking behavior of ice particles to smooth and rough surfaces? What will be the role of the liquid layer on the ice particle?
3. How can the DEM be employed to simulate macroscopic behavior of snow utilizing a micro-mechanical model?

1.2 Literature review

Ice is the constitutive material of the dry snow. Yet, the mechanical properties of snow are much different from that of ice because the structural arrangements of ice particles play an important role in the overall mechanical properties of snow. Ice crystals can have different architectures to form the snow as an open-cell cellular structure. Since snow is a cellular structure, it is highly compressible [2,3]. Consequently, to understand the mechanical behavior of snow it is necessary not only to understand the mechanical behavior of ice but the way the ice particles "engage" to form the snow.

For wet snow, water is also present along with the ice. The nature and behavior of wet snow while significantly different of that of dry snow still widely depends on the amount of water. The analysis of the wet snow is also more complicated since it is more thermodynamically active than the dry snow and needs to be modeled as a multi-phase compound [4]. Wet snow can be thought of a fluidized solid though [5] or a granular material. The change and growth at snow crystals at different environmental conditions is called ***metamorphism***. The scientific definition of snow, despite its palpable nature, might vary based on the point of view. For instance, snow might be defined as “a fine-grained material with a high-specific surface area which is generally at or close to its melting temperature and hence it is very active thermodynamically” [4]; or, as “a cellular form of ice with open cells” [6]. Coherent deposited snow might be defined as “quasi-homogeneous sintered compact of ice grains” [5]. The focus of the current study is on the mechanics of dry snow.

In everyday life, ice is almost always exists near its melting point. A thin Quasi Liquid Layer (QLL) is known to exist on its surface which gives rise to some exotic behaviors like causing ice particles to stick together quickly when they are brought into contact [7–9] or to slipperiness of ice surface when we are skiing [10]. The force required to separate ice particles which stuck together is called the ***sintering*** force [8]. Snow behavior can be understood better if the sintering behavior of ice is deciphered. Understanding ice sintering also helps to get knowledge about ice friction and sliding [11] as well as phenomena like

snow avalanches [12–14]. Ice sintering studies can be helpful in other fields like planetary sciences [15, 16], glaciology and snow ductile-brittle fracture [17], metamorphism [18], as well as cold region engineering [16]. As mentioned, ice sintering can be related to the presence of a liquid layer on the ice surface [8, 19]. Thompson in 1850 (see detailed description in [10]) related this ice sintering phenomenon to the pressure melting which says that the melting point drops due to the applied external pressure as predicted by the Clapeyron equations in thermodynamics [20]. His theory dominated the scientific society for long but the current consensus is that the Faraday's liquid layer freezing [21] effects is the dominant. Michael Faraday [22] was the first to propose the idea of the presence of a thin liquid layer on the surface of ice particles.

Faraday's idea about the presence of a thin liquid layer on the ice surface was a source of controversies for decades, but it is widely accepted now and has been proven by many researchers, e.g. [8, 23]. Indeed, the breakage of the hydrogen bonds results in a jelly layer or QLL on the ice surface at temperatures below the melting point which makes the surface flow possible [24]. The QLL has been extensively investigated by using different experimental methods like X-ray diffraction, X-ray absorption, or ellipsometry [25–33]. More recently, the QLL has been studied theoretically by using Molecular Dynamics (MD) simulation methods [24] and Monte Carlo simulations [34]. A thorough review about the premelting of ice and the QLL on ice has been provided by Slater and Michaelides [35].

The presence of the QLL on the ice surface has a multitude of implications and a strong effect on the friction of ice and snow. Further, the QLL plays a crucial role in phenomena like ice sintering [8, 36] or snow metamorphism [37]. In addition, it has been suggested that the QLL has a strong effect on the chemical concentrations behavior in snow [38]. Despite recognizing the importance of the QLL, it has been alleged that the lack of quantitative or even qualitative observations about the QLL prohibits it to be related to the crystallization of snow [39]. The sublimation condensation caused by the Kelvin effect was proposed as the limiting factor for isothermal snow metamorphism [37], but surface diffusion is also suggested as a strong candidate [40, 41]. Experimentally, surface diffusion was identified as the driving mechanism in ice sintering [40]. Surface diffusion was also found to be the dominant mechanism in snow metamorphism under isothermal conditions; however, for temperatures near the melting point, the sublimation deposition is considered to be the main mechanism [41]. Fluid flow was identified as the dominant mechanism for relative humidities higher than 62% while for relative humidities lower than 37% the diffusion effects were more important [42].Recently, it was shown using theoretical simulations that advective fluxes play an important role in dynamics of the QLL and lubrication formulation was used to model it [43]. The variation and formation of this liquid layer as a function of temperature has been studied using states of the art numerical methods and it was explained how the disordering of the topmost ice surface governs the slipperiness of the ice surface [44, 45].

In 1954, Jensen (see page 26 in [46]) indicated experimentally as the ice becomes colder the sintering force becomes exponentially smaller. The form of the dependence followed

an Arrhenius form and has been used in ice studies to commensurate the results between different temperatures [8, 47]. Kingery [40] measured sintering forces for ice particles in the size range 0.1-3 mm generated in liquid oxygen or nitrogen. The particles were brought together "lightly" and it was shown that pressure melting is not essential for the welding of the ice particles but the surface water diffusion is. Neck radius was shown to increase with both the time and the particle size. Moreover, the temperature dependence was found to follow an Arrhenius equation, but the estimated activation energy is much higher than the value commonly acknowledged today. Gubler [48] conducted a series of measurements and obtained an ice sintering force for the initial state of sintering for time scales between 1-500 seconds. In 2003, Fan et al. [49] experimented micrometer-sized ice particles, which were put together gently, and measured the developed sintering force over time. The main conclusions were that ice sintering occurs even without external pressure, and that this sintering force increases with both time and particle size. In another study in 2007, Szabo and Schneebeli [8] tested two ice cones under a constant external pressure and measured the sintering force for the duration of less than a second while keeping relative humidity around 50%. They also predicted the sintering force for the same particle size when the external force varied from small to larger values. They found both experimentally and analytically that ice particles stick to each other in less than a second even when the contact load and durations are very small.

Analytically, Colbeck [50] developed a formula for the rate of bond growth based on the assumption that the bond neck is groove-shaped and obtained a closed-form solution for the force. However, the final formula is difficult to use since it depends on parameters like liquid layer thickness on the surface of ice particles which are not accurately known. A simple formulation was also developed by Szabo and Schneebeli [8]. However, their assumptions of a constant strain-rate versus time for the initial sintering stage, ignoring stress concentration factor for the fracture load calculation, and application of Hertzian contact theory are questionable. Although previous studies provide much insight into ice sintering, there are some points requiring a unified investigation. For instance, in the work of Fan et al. [49] there was no contact force reported during the sintering, while in the work of Szabo and Schneebeli [8] there was no particle size variation. A study that considers all relevant variables experimentally and provides a simple and applied theoretical framework is lacking in the literature.

In general, a capillary bridge can be formed between particles due to contamination, adsorption, or lubrication [51] and this effect is responsible for the adhesion of small particles. This phenomenon occurs at a relative pressure (or humidity) above 0.3 [52] and is related in most applications to the Kelvin effect when the pore sizes are in nano scale [53–55]. Water vapor can even condensate in the pores at temperatures below the freezing point to form a liquid bridge. This phenomenon has been studied for the case of hydrocarbons and related to the Kelvin effect for pore sizes in the nano meter order [56].

Surface characteristics of the ice and the defects and dislocations are known to highly affect the onset and characteristics of the QLL [35]. Moreover, the presence of asperities,

as for a rough surface, alters or even hinders the formation of the capillary bridge [57]. For instance, it has been indicated that rougher surfaces are more slippery due to the suppression of the capillary adhesion [54]. [58]. The surface roughness is also thought to have an effect on the formation and characteristics for the liquid bridge between the grains [58]. The primary question about the QLL is about the minimum formation temperature and about the temperature dependency of the thickness of the QLL. There is a large discrepancy in the reported experimental results and MD simulations suffer from shortcomings like considering simplified structures and approximate molecular interactions [35]. Consequently, the problem of the thickness of the QLL and its onset is still an attractive question.

The DEM is a simulation method which is mostly used to simulate particulate fluids, granular solids or similar media. It can even be employed to model conventional solids using bonded particles. Having said that, problems like fracture which are difficult to model using the Finite Element Method (FEM), because of the inherent continuity assumption, can be solved using DEM. The DEM is a computationally expensive method since many particles must be treated separately. Dry snow is a an aggregate of ice particles structured in a cellular form and it is this cellular form which lends snow properties like high compressibility. The DEM is one of the tools used to simulate the behavior of dry snow since it allows for dealing with the heterogeneous behavior of the material and phenomenon like particle rotations which otherwise is impossible or difficult in more conventional methods.

One of the problems that can be studied using the DEM is particle packing. Particle packing has been the subject of interest of numerous studies [59–64]. Random Closed Packing (RCP) is useful in characterizing amorphous solids like polymers and thick or supercooled liquids [64] and has been of interest of many researchers since it refers to the upper bound density achievable for mono-sized particles without introducing crystalline arrangements [60, 65]. Random Loose Packing (RLP), on the other hand, refers to a lower possible bound when the deposition is conducted in such a way that the kinetic energy of the particle is dissipated [60].

Young's modulus [66] and strength [67] of granular materials are functions of their density, and many granular materials like snow have a variable density along depth of deposition [68]. Consequently, the determination of density variations in granular materials are of interest in determining the macroscopic strength of the deposition. The DEM is one of the methods used in simulating granular materials with large number of particles [69–78]. The DEM is also widely used in simulations related to snow mechanics [79, 80]. One of the most important steps in DEM is how to generate the initial arrangement of particles to properly mimic the physics. Particles can be generated either collectively or sequentially in DEM. In one collective approach, particles are generated to occupy a space and minimize gaps via mathematical algorithms [61, 64, 81]. In this context, algorithms were also proposed for non-spherical particles [82]. In another collective approach, particles might also be loosely juxtaposed in a container and further pushed via a moving surface to form a dense packing [62]. In a similar collective approach, particles are generated randomly such

that they have a large overlap that later is reduced via relaxation [63] or evolution [59] methods. In the sequential approach, particles are thrown into a container under the application of gravity or reduced gravity [60] from a hopper or feeder. The sequential approach was adopted in this investigation. The achievable density during sequential deposition can be affected by factors like fall speed, inter-particle frictions, and adhesion forces like Van der Waals forces [60, 65, 83]. The effects of fluid forces like Stokes force or Buoyancy on the RLP of the granular materials have also been investigated [60, 65].

For the latter, fluid properties, and long-range forces like hydrodynamic forces play an important role [84]. Even for spherical particles with the same mass density but different materials, the experimental packing density is different because of the different contact properties of the different materials [60]. It has been demonstrated via DEM simulations that introducing friction and adhesion decreases the RLP density [85]. DEM simulations have further shown that by changing the ratio of hard-viscous to soft particles ratio the overall behavior of the granular media can jump from a fluid to a solid like behavior [83]. Conclusively, a dozen of parameters affects the RLP density. Gundlach et al. [86] used sequential filling to fill micrometer-sized ice particles and the packing behavior was studied experimentally for ice particles .

In the case of ice and snow, similar to other granular materials, natural parameters including fall velocity, and bond strength, along with the stickiness affect the density during natural RLP. Further, temperature is always involved since it affects the Young's modulus, bond growth, and bonds strength. For mono-sized rounded particles a hexagonal lattice arrangement achieves the highest possible density. However, in nature, particles have in general different sizes, and a spread in size distribution affects packing density strongly [81, 87]. Moreover, most particles, including snow, are naturally non-spherical; therefore, it is desired to simulate irregular particles in DEM. Generally, two avenues are paved to treat irregular particles in DEM; one is based on ellipsoids or some polygons and the other route uses agglomerates of bonded spheres/disks. For instance, snow particles can take a plethora of shapes [88], which can be modeled by including bonds between particles [79, 80]. If the second approach is chosen, bond modeling is required. To model bonded or cohesive granular materials, traditionally a compact spring model has been used [75, 89–94]. Despite its wide application, the bending-shear coupling is neglected in most cases. A more sophisticated approach is to employ beam Finite Elements (FE) to represent the bonds [70, 83].

1.3 Thesis layout

The motivation and literature review is covered in the current chapter (Chapter 1). The experimental and simulation methods are discussed in Chapter 2. Selected results of the experiments and simulation are presented in Chapter 3. Finally, a summary of the work and future work is discussed in Chapter 4. The papers related to this work is attached to the end of this thesis. The papers published in connection to this thesis are attached to the thesis in the end. That is the road chosen in this thesis.

2 Methods

Two sets of experiments were conducted on the ice particles. In the first set of experiments, the objective was to quantify the dependence of the sintering force to different parameters including temperature, time, pressing force, and size. In the second set of experiments, the aim was to shed some light on the nature of the liquid layer on the ice particle. In addition to the experiments, DEM simulations were conducted for the filling of bonded particles, representing snow, in a container. In what comes next, the experimental and simulation methods are described in more details.

2.1 Ice sintering force

The experiments are phenomenologically presented in Figure 1. The setup was installed in a freezer (item 10 in Figure 1) with achievable minimum temperature of -20°C. A light source (item 1) was used along with a diffuser plate (item 2) to illuminate the ice sample (item 3). Two cameras (items 4 and 6) recorded the images during the experiments. A hygrometer (item 5) measured both the temperature and the relative humidity. A controller (item 7) controlled the movement of the load cell so that the ice particle come together and detach with a constant velocity. A Proportional-Integral-Derivative (PID) controller (item 8), controlled the temperature variations in the freezer. The measured data are transferred to a computer (item 9) for processing. More details on the experimental setup can be found in Paper A at the end of the thesis.

Two ice particles of radii r and R, shown in Figure 2a , were pressed against each other by a force $F(t)$ during a given time duration, t_f. A typical force history is indicated in Figure 2b. As a result of the contact, the contact radius will grow to a final size a_f and

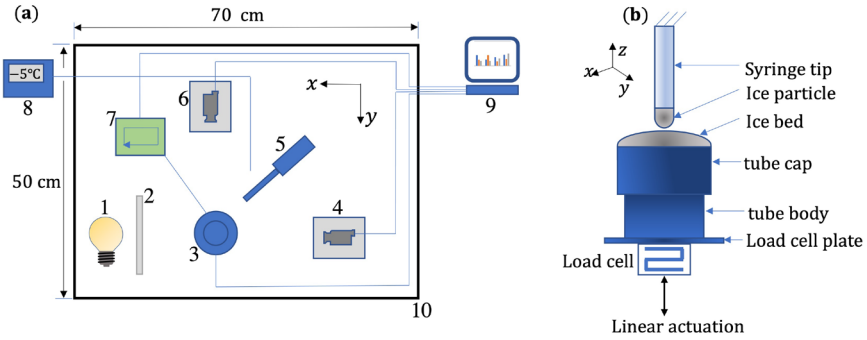

Figure 1: *Layout of the experimental setup for ice sintering force measurement*

the corresponding bonding force F_{sint} is measured as the force needed to break up the bond. The two ice particles are brought into contact during time t_{load}, kept in contact during time t_{keep}, and are separated during the time t_{unload}. During the contact, a bond forms between the ice particles; consequently a tensile force is required to separate them. The aim was to measure this tensile force which is called the sintering force, as depicted in 2b. The temperature, pressing force, $F(t)$, particle radius, r, and contact duration, t_{keep}, were varied and the effects on the sintering force were measured.

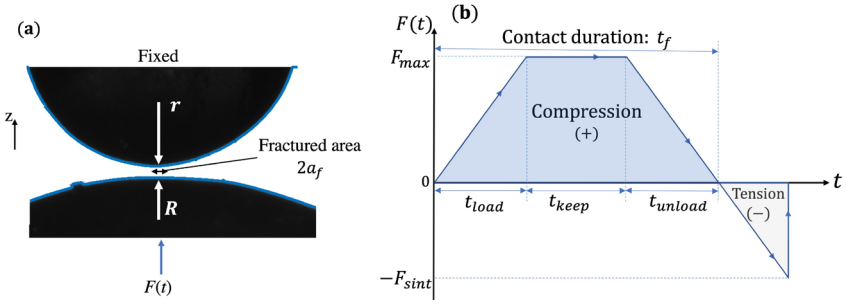

Figure 2: *(a) Geometry of ice particles after contact, (b) Force $F(t)$ imposed on the ice particles to press them*

2.2 Liquid layer on the ice

The experimental setup which is used to study the liquid bridge formation during the contact of an ice particle (with radius $r_{ice} \approx 5$ mm) with a metallic surface is similar to the one used in section 2.1 but some modifications were made to the setup. The upper ice particle is replaced with an Aluminum smooth (or rough) surface so that the contact of the ice to the surface can be experimented. Moreover, a Peltier element was attached to

the back of the Aluminum surface to control the temperature of the surface precisely to have a negligible temperature gradient between the ice particle and the surface. Finally, thermo-couples were used inside the ice, near the Aluminum surface, and in the air to measure the temperatures. The experiments are schematically presented in Figure 3. The detailed description of the setup is provided in Paper B attached to the thesis.

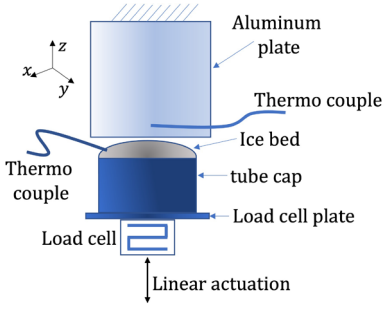

Figure 3: *Experimental setup for observing the liquid bridge between ice and Aluminum*

To study the contact of ice particle with a smooth surface, an Aluminum surface with the mean square roughness of $S_q = 76$ nm was used. It was observed that a liquid bridge was formed during the contact of the ice particle to the smooth Aluminum surface. This liquid bridge stretched and broke during the separation of the ice particle from the surface under controlled velocity. However, when a rougher Aluminum surface with the mean square roughness of $S_q = 272$ nm, was used this liquid bridge did not form in a visible manner during the contact of the ice particle and the Aluminum surface. The layout of the observed liquid bridge is schematically depicted in Figure 4.

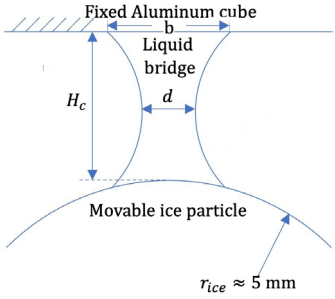

Figure 4: *Layout of the observed liquid bridge during the contact of the ice particle to a smooth Aluminum surface*

There can be multiple reasons for the formation of this liquid bridge during the contact of the ice particle and the smooth Aluminum surface. These can include pressure melting, frictional melting, and Vapor-deposition of what is called the Kelvin effect. Pressure

melting can be rules out since using the Johnson–Kendall–Roberts (JKR) theory, the amount of normal contact stress for the applied forces and given geometries can be found to be around 1 MPa but according to the Clapeyron equation [20], a compressing stress of around 13.5 MPa is required to lower the melting point by one degree. Frictional melting is also not a reason for the melting and formation of the liquid bridge since the contact is only a normal contact and the effects of friction are negligible. The Kelvin effect [56,95,96] is dominant when the gap distance is very small as given by the equation,

$$p/p_0 = \exp\left(\frac{\gamma V_m}{r_{av}\bar{R}T}\right) \tag{1}$$

where, p, p_0, γ, V_m, r_{av}, R, and T are pressure, saturation pressure, work of adhesion, molar volume, equivalent radius, universal gas constant, and temperature, respectively. Using an approximate work of adhesion of 0.85 [97] N/m, molar volume 18 cm^3, gas constant 8.314 J/mol-K, and temperature of 263 K, it can be verified that r_{av} can range from around 6-600 nm for relative humidities of 0.3 to 0.99, respectively. The larger of the obtained radii then is around ten times smaller than the observed radius in these experiments (table 1 in Paper B). Therefore it can be concluded that the Kelvin effect cannot be the dominant mechanism in the formation of the liquid bridge under the conditions considered in this study. The observed liquid bridge between the ice particle and the smooth Aluminum surface was therefore attributed to the presence of a liquid layer on the ice particle and the thickness of this layer was estimated using the observed volume of the liquid bridge:

$$t_{lq} = \frac{H_c}{12}\left[\left(\frac{d}{r_{ice}}\right)^2 + 0.5\left(\frac{b}{r_{ice}}\right)^2\right]. \tag{2}$$

There is a theoretical solution for the dependence of the dimensionless height of the bridge ($H_c^* = H_c/r_{ice}$) to its dimensionless volume ($V_c^* = V/r_{ice}^3$) in the form of, [98]

$$H_c^* \approx V_c^{*1/3}, \tag{3}$$

The thickness of the QLL can be estimated by equating the volume of the liquid bridge to the volume of the thin film on the ice particle. Assuming a semi-spherical shape for the ice particle, the volume of the QLL, V_{lq}, on the ice particle becomes,

$$V_{lq} = 2\pi {r_{ice}}^2 t_{lq}. \tag{4}$$

More details about the methods related to the measurement of the liquid bridge and to the liquid layer on the ice can be found in Paper B attached at the end of the thesis.

2.3 DEM programming

A DEM program was developed in MATLAB (2020a, Mathworks Inc, Natick, MA) to simulate the filling behavior of bonded particles, representing the dry snow. More details can be found in Paper C attached to the end of the thesis.

The first step in the DEM programming is to get or generate particle data like coordinates and radii. As discussed in chapter 1, this can be achieved either by a sequential or a collective approach. In this study, a sequential approach was used since the filling process is of interest. After having the particle data, the general algorithm of the DEM is a loop over time increments to solve for contact forces and update the particle positions. At a specific time step, the following operations must be conducted:

1. Finding possible collisions for each particle,
2. Solving for the collision forces,
3. Solving for bond forces and check bond breakage,
4. Updating the acceleration, velocity, and location.

The collision detection step is the most computationally expensive part. If there exists N particles in the simulation and collision detection is done by brute force method by checking possible collision against all $N-1$ particles, then the algorithm will be $O(N^2)$. To overcome this difficulty, different algorithms are developed which Verlet list and Linked cell methods are the two mostly used ones [99]. In the linked cell method, the whole area or volume is divided into some sub areas or sub volumes and each particle is assigned to a cell. Using this method, to find the possible collisions for a specific particle it is sufficient to check the particles in the neighboring cells instead of checking all the particles. Thus, for mono-dispersed particles, the algorithm is turned to $O(N)$.

The Linked cell method is used in this study and is elaborated below. The explanations is for a two dimensional simulation case, but extension to three dimensions is straightforward. As presented in Figure 5, the whole area is divided into smaller cells and each particle is assigned to a cell. If, for instance, it is of interest to check for possible collisions for particle number 1 in 5, only the particles in the neighboring cells should be checked. In this case, only particles number 2, 3, 4, and 5 should be checked for a possible collision against particle 1. The ideal size of the cell is the size of a particle in the case were particles are mono dispersed. If particles have different sizes then the cell size must be considered to cover the largest particle in the simulation. If the size of the particles are very different, then this algorithm becomes less effective since many particles can be located within a single cell. The Linked Cell method then approaches $O(N^2)$.

Spherical particles with an initial size distribution, shown in Figure 6, were generated using a random distribution algorithm with diameter $d = 250 + 500\ \boldsymbol{\beta}(5{,}10)\ \mu$m, where $\boldsymbol{\beta}$ is the beta-distribution [100]. Particles were considered as bonded and the bonds can break under certain stress conditions.

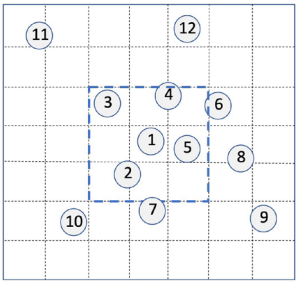

Figure 5: *Description of the Linked cell method in the DEM*

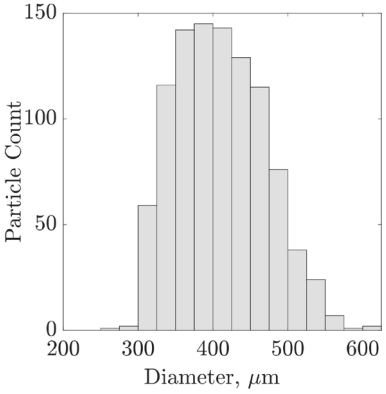

Figure 6: *Particle size distribution used in the DEM simulations*

Normal forces are usually considered as Hertzian forces in the DEM. The presence of frictional forces and moments require more computational resources. Consider the geometry sketched in Figure 7. At any time t, the normal force, ${}^tF_n$, frictional force, ${}^tF_s$, and rolling moment, ${}^tM_r$, can be calculated as,

$$ {}^tF_n = K_n|\min(0,\delta)|^{1.5} + |\min(0,\delta)|\dot{\delta}\eta_n/|\delta| \tag{5} $$

$$ {}^tF_s = -\min\left(K_s \int_0^{\Delta t_{cd}} \Delta V_s(\tau)\, d\tau - \eta_s \Delta^t V_s, \mu_{st}|{}^tF_n|sign(\Delta^t V_s)\right) \tag{6} $$

$$ {}^tM_r = -r\,{}^tF_s - K_r r sign({}^tV_r) \int_0^{\Delta t_{cd}} \Delta V_r(\tau)\, d\tau \tag{7} $$

where, Δt_{cd} is the contact duration, "sign" is the signum function; r is the radius of the particle; η_n and η_s are the normal and tangential damping coefficient, respectively; K_n, K_s, and K_r are normal, tangential, and rolling stiffness values, respectively. The expressions for K_s, and K_r can be found in [101]; ΔV_s is the relative tangential velocity in direction s of the local $n-s$ coordinate system; μ_{st} is the static friction coefficient; δ and $\dot{\delta}$ are normal penetration and normal penetration speed, respectively. Finally, τ is a free integration variable. Relative slip and angular velocities ΔV_s , ΔV_r between particles I and J can be expressed as,

$$ \Delta V_s = {}_IV_s - {}_I\omega_I r - {}_JV_s - {}_J\omega_J r \tag{8} $$

$$ \Delta V_r = {}_I\omega - {}_J\omega \tag{9} $$

The time step, dt, is a critical parameter to maximize the calculation efficiency while maintaining the numerical stability. In this study, the time step is considered to be a fraction of the critical time step in the system, and is defined as,

$$ dt = 2.9\alpha_t \sqrt{\frac{m_{min}}{K_{max}}} \tag{10} $$

where, m_{min} is the mass of the smallest particle in the system; K_{max} is the maximum stiffness in the system, and $\alpha_t = 0.025$ or 0.2, for bonded and non-bonded cases, respectively.

2.3.1 Bonding between particles

The bond between the particles can be modeled using simple linear or rotational (or torsional) springs but generally the coupling effects will be lost. A more sophisticated approach is to use a beam element connecting center-center of the particles. The stiffness of this beam element can be calculated once the diameter of the beam is known. On the other hand, the modeled beam element can break under a certain stress or strain. The value of the breaking stress can be obtained using the calculated sintering force between the ice particles (see section 3.1).

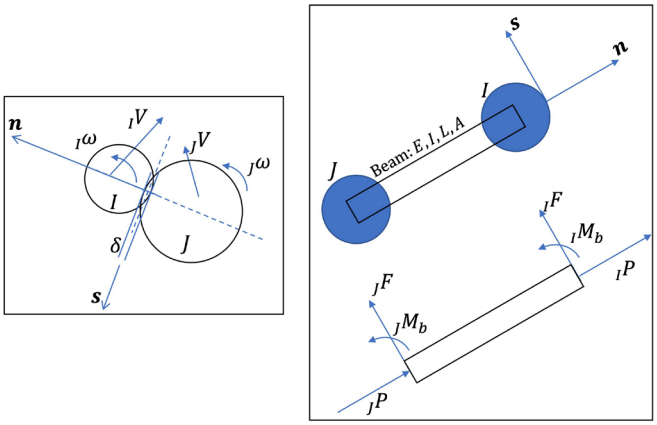

Figure 7: *Particles in collision (left), bond model (right)*

Timoshenko beam elements connecting center-center of particles are used to model the bond element, as depicted in Figure 7. Since at every time step, particles move only a tiny amount, the assumption of large displacement with small deflections are applicable which made it possible to use an incremental method keeping the tangent matrix as a constant [102] in accordance with previous works [70, 83]. The incremental bond force is defined as,

$$^{t+dt}F_{bond} = {}^{t}F_{bond} + K_{beam}V_{bond}dt \tag{11}$$

where, K_{beam} is the ordinary Timoshenko beam stiffness element, which can be found in any finite element book [103], and V_{bond} is the beam nodal velocity vector of the beam. Details can be found in paper C attached to this thesis.

The Coulomb-Mohr criterion is used to identify the bond failure loads [104], as,

$$\frac{\sigma_1}{S_{ut}} - \frac{\sigma_3}{S_{uc}} \geq 1 \tag{12}$$

where, S_{ut} and S_{uc} are tensile and compressive strength of ice, respectively. S_{ut} (see paper C attached to the thesis) and S_{uc} is taken as $5S_{ut}$. Note that S_{uc} is much larger than S_{ut} for ice, like for many other brittle materials [6]. σ_1 and σ_1 are the maximum and minimum principal stresses which can be obtained using the axial, bending, and shear loading of the beam element.

2.3.2 Updating positions

After calculating the forces, it is straightforward to obtain the linear or angular accelerations by dividing the force by the inertial terms. The velocities and positions of the particles in the next time step can be obtained using simple integration over the time step as:

$$^{t_i+0.5dt}v = {}^{t_i}v + {}^{t_i}adt/2 \tag{13}$$

$$^{t_{i+1}}x = {}^{t_i}x + {}^{t_i+0.5dt}vdt \tag{14}$$

$$^{t_{i+1}}v = {}^{t_i+0.5dt}v + {}^{t_{i+1}}adt/2 \tag{15}$$

where, x, v, and a represent displacement, velocity, and acceleration vectors; left superscripts represent the time, and dt is the marching time from Eq 10. Similar formulas are used for angular velocities and rotations. Ice particles are generated using a beta-distribution, with the possibility to bond the particles together in the beginning, before inserting them into the container area. However, they may also be bonded which is the topic of the next section.

3 Results

In this chapter, a semi-analytical, closed form formulation for the sintering force of the ice particles are presented in Section 3.1. in section 3.2, the results from experiments related to the ice sintering force and liquid layer on the ice are also presented. In addition, in section 3.3, the DEM simulation results for filling of a container with bonded particles are presented.

3.1 Sintering force of ice

The initial neck diameter that forms during the sintering of ice particles can be approximated using the JKR model and the subsequent growth can be estimated using the existing experimental data for the first-stage creep of the ice. In this way, the neck radius can be expressed as,

$$a_f = \left\{ \left(\frac{9\pi W R^{*2}}{2E^*} \right)^{\frac{2(1+m)}{3}} + 2C_0 R^{*2}(1+m){F_{max}}^m \left[\frac{t_l^{1-\beta}}{(1+m-\beta} + \right. \right.$$
$$\left. \left. \frac{(t_l+t_k)^{(1-\beta)} - {t_l}^{(1-\beta)}}{(1-\beta)} + (\frac{t_f}{t_u})^{(1+m-\beta)} {t_u}^{(1-\beta)} (\mathbf{B_1}(1-\beta, 1+\alpha) - \mathbf{B}_{\mathbf{1-\frac{t_u}{t_f}}}(1-\beta, 1+\alpha)) \right] \right\}^{\frac{1}{2(1+m)}} \tag{16}$$

where, R^* is the equivalent radius, W is the work of adhesion, E^* is the effective modulus, a_f is the bond radius at the end of unloading, t_f; $C_0 = 1.204 \times 10^{-20}$, m = 2.43, and

$\beta = 1/3$. Also, $t_l \equiv t_{load}$, $t_k \equiv t_{keep}$, $t_u \equiv t_{unload}$, and $\mathbf{B}$ is the incomplete beta function defined in [105],

Once the neck radius is determined, the force required for the fracture of ice in tension can be obtained. Since ice is a brittle material, a stress concentration factor should be included in the formulations. A ratio of $S_{ut}/K_s = 1.1$ MPa was found to well present the sintering force value for the experimented conditions. The obtained force can be scaled with the temperature using Arrhenius equation, and activation energy of the ice can be obtained. Considering,

$$F_{sint}(T, F, R^*, t_f) = \pi e^k \left(\frac{S_{ut}}{K_s}\right) a^2(F, R^*, t_f), \tag{17}$$

the sintering force is obtainable from Eq. 16, as,

$$F_{sint} = \left(\frac{S_{ut}}{K_s}\right) \pi e^k \left\{ \left(\frac{9\pi W R^{*2}}{2E^*}\right)^{\frac{2(1+m)}{3}} + 2C_0 R^{*2}(1+m){F_{max}}^m \left[\frac{t_l^{1-\beta}}{(1+m-\beta} + \right.\right.$$
$$\left.\left. \frac{(t_l+t_k)^{(1-\beta)} - {t_l}^{(1-\beta)}}{(1-\beta)} + (\frac{t_f}{t_u})^{(1+m-\beta)} {t_u}^{(1-\beta)} (\mathbf{B_1}(1-\beta, 1+\alpha) - \mathbf{B}_{\mathbf{1-\frac{t_u}{t_f}}}(1-\beta, 1+\alpha)) \right] \right\}^{\frac{1}{1+m}} \tag{18}$$

where,

$$k = -\frac{Q}{nR_g}\left(\frac{1}{273.15+T} - \frac{1}{268.15}\right) \tag{19}$$

is the exponent of the Arrhenius equation. In Eq. 19 , $Q = 133$ kJ/mol, $n = 3$ and $R_g = 8.314$ J/K-mol is the molar gas constant [19]. In addition, the temperature T is given in ^{o}C in and the reference temperature 268.15 K is included.

The experiments revealed that the sintering force increases with particle size, time, imposed pressure, and decreases with the temperature. The dependence of the sintering force to the particle size and time is exhibited in Figure 8. The dependence of the sintering force to the particle size follows a power law with the exponent of 0.64 which is close to the theoretical value of 2/3 predicted in the sintering theory for the particles [106].

The dependence of the sintering force to the pressing force and to the temperature is presented in Figure 9. From the temperature dependence, the activation energy is obtainable as 41.4 kJ/Kmol. [107].

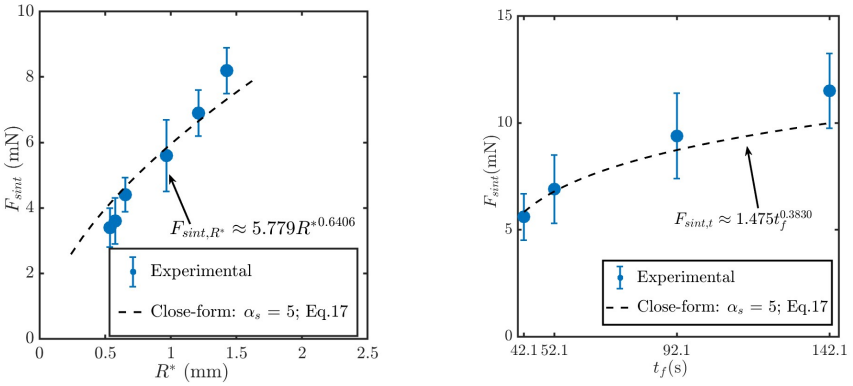

(a) *Sintering force-size* ***(b)*** *Sintering force-time*

Figure 8: *The variations of the sintering force with the particle size and time*

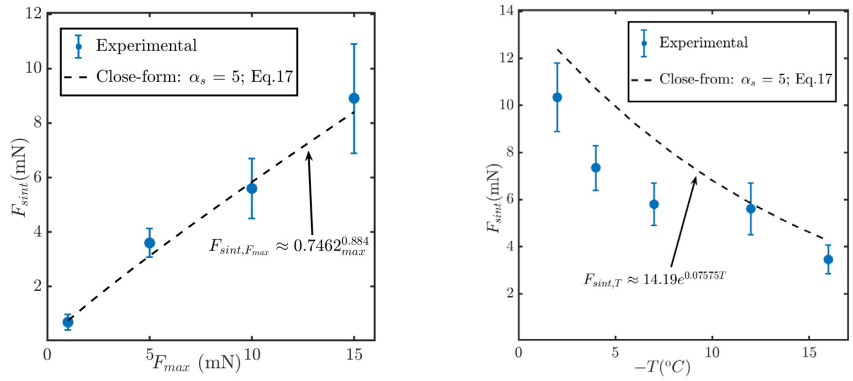

(a) *Sintering force-pressing force* ***(b)*** *Sintering force-temperature*

Figure 9: *The variations of the sintering force with the pressing force and the temperature*

3.2 Liquid layer on the ice

The height of the liquid bridge which is formed in contact of the ice particle with a smooth surface is plotted against its volume in Figure 10a. The volume of the bridge is theoretically expected to increase with its height at separation instant by a power of 1/3, as $V \propto H^{1/3}$. The observed results here verify the theoretical ground and follow the same trend which is observed for hydrocarbons. However, the scales of observation is orders of magnitudes lager here compared to the reported results in [108] for hydrocarbons. The thickness of the liquid layer on the ice particle is plotted in Figure 10b. The thickness of the liquid layer sharply decreases with the temperature as depicted in 10b. The dashed line has the equation,

$$t_{lq} = 172.2(T_M - T)^{-2.59} \tag{20}$$

obtained from regression, where $T_M = 0^{o}$C is the melting temperature, and T is temperature in ^{o}C.

The model we used in this study is an approximate model, and the volume of the liquid film modeled in Eq. 20 is a rough estimation. The weak part of the model is the assumption that the entire liquid film on the ice surface flows into the liquid bridge. Using contact experiments between tipless cantilevers and a silicon wafer on an AFM, the growth mechanisms of a water bridge at different Relative humidities was investigated in [42]. With the aid of potassium hydroxide (KOH) coatings, a "radius of collection" of 23.6 μm was obtained for which the film certainly moves toward the contact area. The cantilever width in [42] was 60 μm The radius in the current experiment is around 5 mm. A linear scaling provides an estimation for the expected radius of collection of $5 \times 23.6/30 \approx 4$ mm which is in the order of the radius of the ice particle. Moreover, since the relative humidity in this study is high enough, $\approx 50\%$, the flow mechanism of the QLL dominates over the surface diffusion effects, as explained in [42], and advective effects are important.

It is most likely that the model underestimate the film thickness in general and in particular for lower temperatures since the fluidity will be less due to the increased viscosity. The film thickness as predicted by Eq. 2 will therefore be a lower bound for the actual film thickness and the power dependence of $(T_M - T)^{-2.59}$ will be an overestimation of the temperature dependence. The relation should therefore be written as $(T_M - T)^{-\beta}$, where $\beta < 2.59$. Determining a correct value for β will require more detailed experiments.

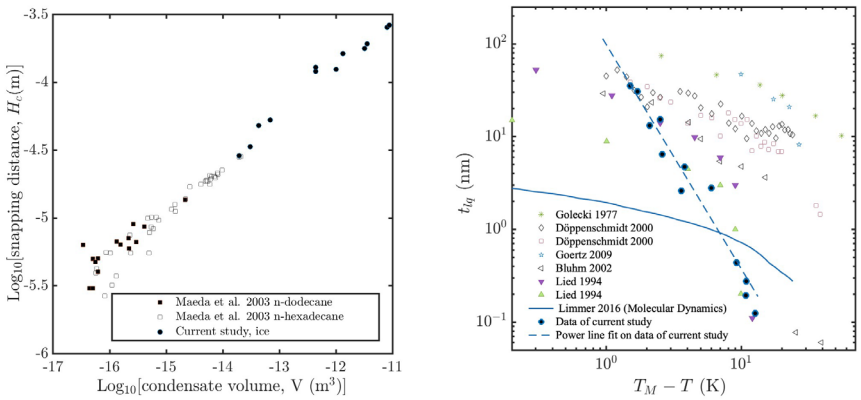

(a) *Height versus volume of liquid bridge* ***(b)*** *Thickness of the liquid layer on the ice*

Figure 10: *Liquid bridge volume versus height and liquid layer thickness on the ice particle*

3.3 DEM simulation

In this section, a summary of the results of the filling of a container with bonded ice particles representing snow is presented. The effect of the drag force on the filling was studied and the angle of repose of snow as a function of temperature was simulated. More details about the simulation results can be found in Paper C attached at the end of the thesis.

As depicted in Figure 11a, deposition of mono-dispersed particles shapes a "preferred"-hexagonal-order, which is the ordered-packing with a preferred highest density arrangement in two dimensional lattices. The compatibility mechanism that allowed the particles to achieve this hexagonal arrangement, is the movement of slip band (shear bands) within the material. Indeed, via geometrically necessary dislocations ([109], the material adopted itself for strain gradients during the filling process to take the shape of the container. Voids are also formed as seen in Figure 11a, which can alter the macroscopic behavior of the material significantly. Adding a perturbation in the size of particles to have nonuniform diameters results in an amorphous configuration as presented in Figure 11b. In these experiments, gravitational acceleration $g = 9.81$ m/s^2 and friction coefficient $\mu = 0.9$ are considered. For experiments with mono-dispersed particles, the corresponding diameter is set to 500 μm and for experiments with poly-dispersed particles the particle diameter varies according to Figure 6.

Since the static friction coefficient for ice can reach to near unity [110,111], and the related static friction force is the force responsible to allow particles to move and rearrange, an increasing friction coefficient must decrease the packing density, as observed in previous

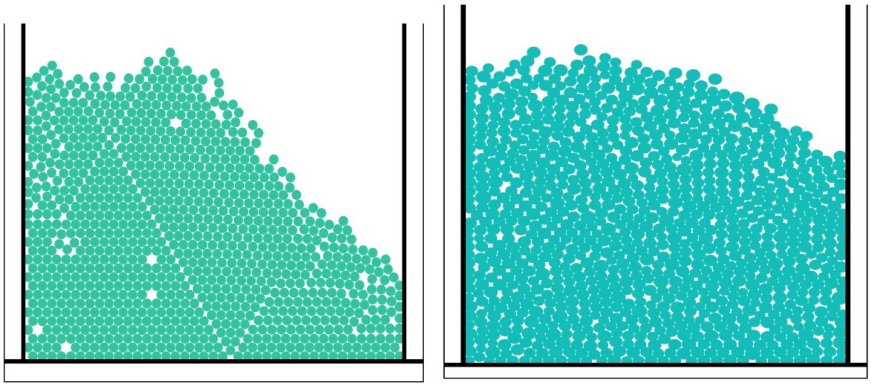

(a) *mono-dispersed particles* ***(b)*** *Multi-dispersed particles*

Figure 11: *filling of non bonded particles*

published works [112]. Moreover, it is known that the density of packing increases with the depth of deposition [113]. Here a set of simulation results for non-bonded poly-dispersed particles and various friction coefficients revealed that the density decreases with increasing friction coefficient and increasing with depth, as presented in Figure 12. Gravitational acceleration $g = 9.81$ m/s^2 is considered.

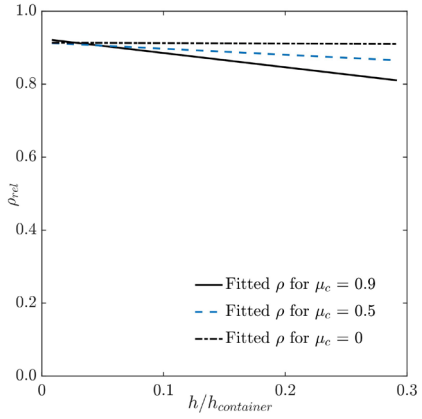

Figure 12: *The effect of the friction coefficient on the relative density variation with the depth of deposition for frictional mono-dispersed particles with diameter 500 μm*

To attain lower rates in the deposition process, it is possible to suspend the particles in a fluidic medium [60, 65]. In this case, due to the movement of particles in the fluid, several forces and moments can be exerted on the particle [101]. For smaller particles, the most important forces are drag forces which can be realized by reduced gravity [101]. Here,

the effect of deposition rate is studied by reducing the effective gravitational acceleration on the particles. When $g_r \rightarrow 0$, particles hit the surface with lower kinetic energy, as presented in Figure 13. It is obvious from this figure that decreasing effective gravity decreases the effective density especially near the surface and increases the irregular pattern depth close to the surface. Gravitational acceleration, $g = \{0.490, 0.981, 9.81\}$ m/s^2 and friction coefficient $\mu = 0.9$ are considered while the particles are kept at the constant diameter of 500µm.

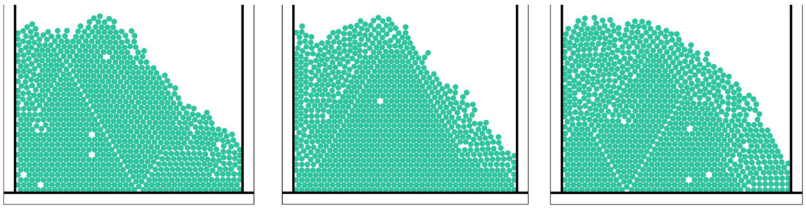

Figure 13: *mono-dispersed particles: no bonding is considered, friction coefficient µ=0.9: g=9.81 (left), g=9.81/10 (middle), and g=9.81/20 (right); particle diameter: 500 µm*

When drag forces according to $F_{drag} = -10\pi V d$ are introduced, where V and d, are velocity and diameter of the particle respectively, it is seen in Figure 14 that as particles fall, they form new bonds, roll over each other and reconfigure in an irregular surface shape, as previously reported [86].

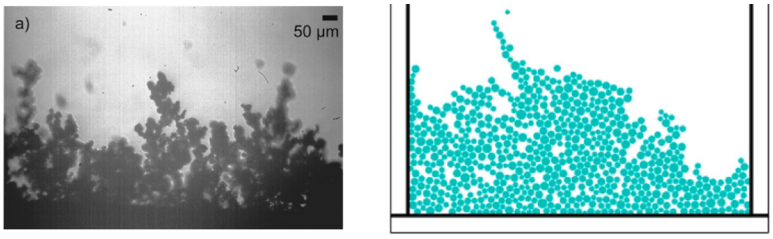

Figure 14: *experimental results of sticky ice particles accumulation from experimental results [86](left); simulated results using DEM (right) F_{drag} = -10π V d*

For a granular material, angles of repose (here for snow) is a function of inter-particle friction, shape, and bond forces [114]. Therefore, checking the model against an experimentally validated macroscopic model is a reliable way to discern that internal parameters of the model work righteously. A typical DEM simulation and them angle of repose, Φ, is depicted in Figure 15a. The measured angle of repose from the simulated packings are compared with the results from [114] and shows good agreement with the experimental results for faceted snow (Figure 15b. In [114], the angle of repose for ice beads are significantly lower which indicates that mono-dispersed particles probably cannot capture the behavior in the best way.

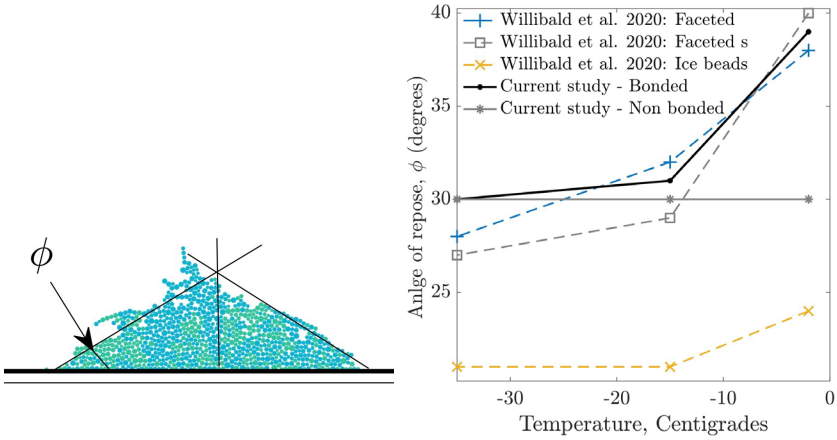

(a) *A typical angle of repose measurement for snow at temperature -1° C* ***(b)*** *Comparisons between angle of repose from this study with data published elsewhere*

Figure 15: *Angle of repose of snow as a function of temperature*

The settings for the simulation results depicted in Figure 15 are: gravitational acceleration, $g = 9.81$ m/s^2; poly-dispersed particle size distribution according to Figure 6; average time step, dt = 0.1 μs; container size (width $\times$ height), $w \times h = 20$ mm $\times$ 60 mm; particles are released with initial zero velocity; Particles are released in the form of bonded linear clusters as depicted in Figure 6 such that the height and horizontal location of the middle particle are 54mm and 30mm, respectively; cluster length is 0.35 of the width of the container ; the bonded cluster has a random inclination between 0 (horizontal configuration for the cluster) to 90° (rotated in clockwise direction); Number of particles, $N_{tot} = 1000$; Poisson's ratio, $\nu = 0.4$; density, $\rho = 917$ Kg/m^3; drag forces are introduced as F_{drag} = -10πV d, where V and d, are velocity and diameter of the particle respectively.

4

Summary & Future work

4.1 Summery

In this work, a series of experiments were conducted on ice in the micro level to understand the micro mechanics of ice cohesion or equivalently the sintering force in more details. From the experiments, the dependency of the sintering force to the particle size, sintering time, applied pressure, and temperature was identified. considering the dependency of the sintering force on the aforementioned parameters, $F_{sint}(T, F, R^*, t_f) = \pi e^k \left(\frac{S_{ut}}{K_s}\right) a^2(F, R^*, t_f)$, a semi-analytic formulation was developed to predict the dependency of the sintering force of ice particles to the aforementioned parameters considering the first-stage creep of the ice particles. The semi-analytic formula was in good accordance with the observed results. Both formulation and experiments showed that the ice sintering force increases with particle size, time and pressure, and decreases with temperature. The latter follows a well known Arrhenius equation from which the activation energy is estimable as 41.4 J/mol-K

Moreover, a set of experiments were conducted in this work to shed some light on the nature of the liquid layer on the ice particle. With approaching an ice particle to a "smooth" surface, a clearly visible liquid bridge was observed during the contact and upon the separation. This liquid bridge stretched until it ruptured when the ice particle moved apart from the smooth surface with controlled velocity. It was hypothesized that the presence of a liquid layer on the ice particle and its advection to the contact area is the reason for formation of the liquid bridge. This hypothesis was used to estimated the thickness of the liquid layer on the ice particle assuming all the liquid can move into the contact area during the contact. This approximation resulted in an estimate for

liquid layer thickness which lies within the previously reported data. The dependent was identified in the form of $t_{lq} = (T_M - T)^{-\beta}$ with $\beta < 2.6$.

With Discrete element simulation on the filling process of bonded particles in a container, the process of filling of snow in a container was simulated. A damped Hertzian force model was used for collision of the non-bonded particles while a Timoshenko beam model was used to model the bonded particles interactions. The dependency of the relative density of the filling to the bonding or indirectly to the temperature was identified. In , the angle of repose of snow as bonded ice particles was

4.2 Future work

The next step in this work is to conduct a series of uni-axial compression tests on a cylindrical snow sample with diameter and height of nearly 1 cm and image the sample using micro tomography technique while it is being loaded. The tests will be conducted for both artificial and natural snow. The objective is to obtain the three dimensional structure and its variation with the loading. The force displacement data will be used to obtain the related nominal stress-strain curves and it will be related to the relative density of the snow which can be obtained from the binary image segmentation of the images. From the force-time curves the nominal stress-time curves will be obtained and then the density-dependent visco-elastic properties of snow at each step will be obtained by using a four-parameter visco-elastic solid model composed of a Voigt-Kelvin and a Maxwell solid in series.

References

[1] C. Hill, "23 state dots spent more than $1 billion on snow, ice maintenance this winter."

[2] A. Stomakhin, C. Schroeder, L. Chai, J. Teran, and A. Selle, "A material point method for snow simulation," *ACM Transactions on Graphics (TOG)*, vol. 32, no. 4, pp. 1–10, 2013.

[3] G. White and A. McCallum, "Review of ice and snow runway pavements," *International Journal of Pavement Research and Technology*, vol. 11, no. 3, pp. 311–320, 2018.

[4] S. Colbeck, "An overview of seasonal snow metamorphism," *Reviews of Geophysics and space physics*, vol. 20, no. 1, pp. 45–61, 1982.

[5] M. Mellor, *A review of basic snow mechanics*. US Army Cold Regions Research and Engineering Laboratory, 1974.

[6] J. Petrovic, "Review mechanical properties of ice and snow," *Journal of materials science*, vol. 38, no. 1, pp. 1–6, 2003.

[7] C. Willibald, J. Dual, M. Schneebeli, and H. Löwe, "Size controls on the crossover from normal to self-inhibited sintering of ice spheres," *Acta Materialia*, vol. 213, p. 116926, 2021.

[8] D. Szabo and M. Schneebeli, "Subsecond sintering of ice," *Applied Physics Letters*, vol. 90, no. 15, pp. 1–4, 2007.

[9] J. R. Blackford, "Sintering and microstructure of ice: A review," *Journal of Physics D: Applied Physics*, vol. 40, no. 21, 2007.

[10] R. Rosenberg *et al.*, "Why is ice slippery?," *Physics Today*, vol. 58, no. 12, p. 50, 2005.

[11] N. Maeno and M. Arakawa, "Adhesion shear theory of ice friction at low sliding velocities, combined with ice sintering," *Journal of Applied Physics*, vol. 95, no. 1, pp. 134–139, 2004.

[12] J. Gaume, A. Van Herwijnen, G. Chambon, N. Wever, and J. Schweizer, "Snow fracture in relation to slab avalanche release: Critical state for the onset of crack propagation," *Cryosphere*, vol. 11, no. 1, pp. 217–228, 2017.

[13] D. Mulak and J. Gaume, "Numerical investigation of the mixed-mode failure of snow," *Computational Particle Mechanics*, vol. 6, no. 3, pp. 439–447, 2019.

[14] A. Capelli, I. Reiweger, and J. Schweizer, "Studying snow failure with fiber bundle models," *Frontiers in Physics*, vol. 8, no. July, 2020.

[15] F. G. Bridges, K. D. Supulver, D. N. Lin, R. Knight, and M. Zafra, "Energy loss and sticking mechanisms in particle aggregation in planetesimal formation," *Icarus*, vol. 123, no. 2, pp. 422–435, 1996.

[16] T. Schultz, R. Müller, D. Gross, and A. Humbert, "Modelling the transformation from snow to ice based on the underlying sintering process," *Pamm*, vol. 20, no. 1, pp. 2020–2022, 2021.

[17] H. Löwe, M. Zaiser, S. Mösinger, and S. Schleef, "Snow mechanics near the ductile-brittle transition: Compressive stick-slip and snow microquakes," *Geophysical Research Letters*, vol. 47, no. 4, p. e2019GL085491, 2020.

[18] A. Van Herwijnen and D. A. Miller, "Experimental and numerical investigation of the sintering rate of snow," *Journal of Glaciology*, vol. 59, no. 214, pp. 269–274, 2013.

[19] V. F. Petrenko and R. W. Whitworth, *Physics of Ice*. Oxford University Press, 2006.

[20] C. Borgnakke and R. E. Sonntag, *Fundamentals of thermodynamics*. John Wiley & Sons, 2022.

[21] M. Faraday, "On regelation, and on the conservation of force," *Philos Mag*, vol. 17, no. 113, pp. 162–169, 1859.

[22] M. Faraday, "I. note on regelation," *Proceedings of the Royal Society of London*, no. 10, pp. 440–450, 1860.

[23] U. Nakaya and A. Matsumoto, "Simple experiment showing the existence of "liquid water" film on the ice surface," *Journal of Colloid Science*, vol. 9, no. 1, pp. 41–49, 1954.

[24] D. T. Limmer, "Closer look at the surface of ice," *Proceedings of the National Academy of Sciences of the United States of America*, vol. 113, pp. 12347–12349, 11 2016.

[25] M. Elbaum, S. Lipson, and J. Dash, "Optical study of surface melting on ice," *Journal of crystal growth*, vol. 129, no. 3-4, pp. 491–505, 1993.

[26] I. Golecki and C. Jaccard, "The surface of ice near 0 c studied by 100 kev proton channeling," *Physics Letters A*, vol. 63, no. 3, pp. 374–376, 1977.

[27] A. Döppenschmidt and H.-J. Butt, "Measuring the thickness of the liquid-like layer on ice surfaces with atomic force microscopy," *Langmuir*, vol. 16, no. 16, pp. 6709–6714, 2000.

[28] M. Goertz, X.-Y. Zhu, and J. Houston, "Exploring the liquid-like layer on the ice surface," *Langmuir*, vol. 25, no. 12, pp. 6905–6908, 2009.

[29] H. Bluhm, D. F. Ogletree, C. S. Fadley, Z. Hussain, and M. Salmeron, "The premelting of ice studied with photoelectron spectroscopy," *Journal of Physics: Condensed Matter*, vol. 14, no. 8, p. L227, 2002.

[30] A. Lied, H. Dosch, and J. Bilgram, "Surface melting of ice i h single crystals revealed by glancing angle x-ray scattering," *Physical Review Letters*, vol. 72, no. 22, p. 3554, 1994.

[31] G. Sazaki, S. Zepeda, S. Nakatsubo, M. Yokomine, and Y. Furukawa, "Quasi-liquid layers on ice crystal surfaces are made up of two different phases," *Proceedings of the National Academy of Sciences*, vol. 109, no. 4, pp. 1052–1055, 2012.

[32] H. Asakawa, G. Sazaki, K. Nagashima, S. Nakatsubo, and Y. Furukawa, "Two types of quasi-liquid layers on ice crystals are formed kinetically," *Proceedings of the National Academy of Sciences of the United States of America*, vol. 113, pp. 1749–1753, 2 2016.

[33] M. A. Sánchez, T. Kling, T. Ishiyama, M.-J. van Zadel, P. J. Bisson, M. Mezger, M. N. Jochum, J. D. Cyran, W. J. Smit, H. J. Bakker, *et al.*, "Experimental and theoretical evidence for bilayer-by-bilayer surface melting of crystalline ice," *Proceedings of the National Academy of Sciences*, vol. 114, no. 2, pp. 227–232, 2017.

[34] I. Pickering, M. Paleico, Y. A. P. Sirkin, D. A. Scherlis, and M. H. Factorovich, "Grand canonical investigation of the quasi liquid layer of ice: Is it liquid?," *The Journal of Physical Chemistry B*, vol. 122, no. 18, pp. 4880–4890, 2018.

[35] B. Slater and A. Michaelides, "Surface premelting of water ice," *Nature Reviews Chemistry*, vol. 3, no. 3, pp. 172–188, 2019.

[36] H. Bahaloo, T. Eidevåg, P. Gren, J. Casselgren, F. Forsberg, P. Abrahamsson, and M. Sjödahl, "Ice sintering: Dependence of sintering force on temperature, load, duration, and particle size," *Journal of Applied Physics*, vol. 131, no. 2, p. 025109, 2022.

[37] P. P. Ebner, M. Schneebeli, and A. Steinfeld, "Tomography-based monitoring of isothermal snow metamorphism under advective conditions," *The Cryosphere*, vol. 9, no. 4, pp. 1363–1371, 2015.

[38] E. Waddington, J. Cunningham, and S. Harder, "The effects of snow ventilation on chemical concentrations," in *Chemical Exchange between the atmosphere and polar snow*, pp. 403–451, Springer, 1996.

[39] K. G. Libbrecht, "The physics of snow crystals," *Reports on progress in physics*, vol. 68, no. 4, p. 855, 2005.

[40] W. Kingery, "Regelation, surface diffusion, and ice sintering," *Journal of Applied Physics*, vol. 31, no. 5, pp. 833–838, 1960.

[41] R. Vetter, S. Sigg, H. M. Singer, D. Kadau, H. J. Herrmann, and M. Schneebeli, "Simulating isothermal aging of snow," *EPL (Europhysics Letters)*, vol. 89, no. 2, p. 26001, 2010.

[42] T. Lai and P. Li, "Direct evidence of a radius of collection area for thin film flow in liquid bridge formation by repeated contacts using afm," *Langmuir*, vol. 35, no. 20, pp. 6585–6593, 2019.

[43] D. N. Sibley, P. Llombart, E. G. Noya, A. J. Archer, and L. G. MacDowell, "How ice grows from premelting films and water droplets," *Nature communications*, vol. 12, no. 1, pp. 1–11, 2021.

[44] Y. Nagata, T. Hama, E. H. Backus, M. Mezger, D. Bonn, M. Bonn, and G. Sazaki, "The surface of ice under equilibrium and nonequilibrium conditions," *Accounts of Chemical Research*, vol. 52, no. 4, pp. 1006–1015, 2019.

[45] B. Weber, Y. Nagata, S. Ketzetzi, F. Tang, W. J. Smit, H. J. Bakker, E. H. Backus, M. Bonn, and D. Bonn, "Molecular insight into the slipperiness of ice," *Journal of Physical Chemistry Letters*, vol. 9, no. 11, pp. 2838–2842, 2018.

[46] P. V. Hobbs, *The sintering and adhesion of ice*. PhD thesis, 1963.

[47] O. S. Toker, S. Karaman, F. Yuksel, M. Dogan, A. Kayacier, and M. T. Yilmaz, "Temperature dependency of steady, dynamic, and creep-recovery rheological properties of ice cream mix," *Food and Bioprocess Technology*, vol. 6, no. 11, pp. 2974–2985, 2013.

[48] H. Gubler, "Strength o f bonds between ice grains after short contact times," *Journal of Glaciology*, vol. 28, no. 100, pp. 457–473, 1982.

[49] X. Fan, P. Ten, C. Clarke, A. Bramley, and Z. Zhang, "Direct measurement of the adhesive force between ice particles by micromanipulation," *Powder Technology*, vol. 131, no. 2-3, pp. 105–110, 2003.

[50] S. C. Colbeck, "Sintering in a dry snow cover," *Journal of Applied Physics*, vol. 84, no. 8, pp. 4585–4589, 1998.

[51] C. Gao, "Theory of menisci and its applications," *Applied physics letters*, vol. 71, no. 13, pp. 1801–1803, 1997.

[52] J.-G. Choi, D. Do, and H. Do, "Surface diffusion of adsorbed molecules in porous media: Monolayer, multilayer, and capillary condensation regimes," *Industrial & engineering chemistry research*, vol. 40, no. 19, pp. 4005–4031, 2001.

[53] M. V. Vitorino, A. Vieira, C. A. Marques, and M. S. Rodrigues, "Direct measurement of the capillary condensation time of a water nanobridge," *Scientific Reports*, vol. 8, 12 2018.

[54] F.-C. Hsia, S. Franklin, P. Audebert, A. M. Brouwer, D. Bonn, and B. Weber, "Rougher is more slippery: How adhesive friction decreases with increasing surface roughness due to the suppression of capillary adhesion," *Physical Review Research*, vol. 3, no. 4, p. 043204, 2021.

[55] I. Deroche, T. J. Daou, C. Picard, and B. Coasne, "Reminiscent capillarity in subnanopores," *Nature Communications*, vol. 10, 12 2019.

[56] D. Nowak and H. K. Christenson, "Capillary condensation of water between mica srfaces above and below zero-effect of surface ions," *Langmuir*, vol. 25, pp. 9908–9912, 9 2009.

[57] C. Xiao, P. Shi, W. Yan, L. Chen, L. Qian, and S. H. Kim, "Thickness and structure of adsorbed water layer and effects on adhesion and friction at nanoasperity contact," *Colloids and Interfaces*, vol. 3, no. 3, p. 55, 2019.

[58] S. Herminghaus, "Dynamics of wet granular matter," *Advances in physics*, vol. 54, no. 3, pp. 221–261, 2005.

[59] R. S. Farr and R. D. Groot, "Close packing density of polydisperse hard spheres," *Journal of Chemical Physics*, vol. 131, no. 24, pp. 1–8, 2009.

[60] G. R. Farrell, K. M. Martini, and N. Menon, "Loose packings of frictional spheres," *Soft Matter*, vol. 6, no. 13, pp. 2925–2930, 2010.

[61] K. Han, Y. T. Feng, and D. R. Owen, "Sphere packing with a geometric based compression algorithm," *Powder Technology*, vol. 155, no. 1, pp. 33–41, 2005.

[62] B. D. Lubachevsky and F. H. Stillinger, "Geometric properties of random disk packings," *Journal of Statistical Physics*, vol. 60, no. 5-6, pp. 561–583, 1990.

[63] L. Meng, Y. Jiao, and S. Li, "Maximally dense random packings of spherocylinders," *Powder Technology*, vol. 292, pp. 176–185, 2016.

[64] A. Z. Zinchenko, "Algorithm for random close packing of spheres with periodic boundary conditions," *Journal of Computational Physics*, vol. 114, no. 2, pp. 298–307, 1994.

[65] K. J. Dong, R. Y. Yang, R. P. Zou, and A. B. Yu, "Role of interparticle forces in the formation of random loose packing," *Physical Review Letters*, vol. 145505, no. 96, 2006.

[66] H. Bader, "Special report 64 density of ice by," Tech. Rep. August, Hanover, NH, 1964.

[67] M. P. Schöpfer, S. Abe, C. Childs, and J. J. Walsh, "The impact of porosity and crack density on the elasticity, strength and friction of cohesive granular materials: Insights from dem modelling," *International Journal of Rock Mechanics and Mining Sciences*, vol. 46, no. 2, pp. 250–261, 2009.

[68] D. L. Anderson and C. S. Benson, *The densification and diagenesis of snow. In: Ice and Snow: Properties, Processes and Applications.* Cambridge, MA: MIT Press, 1963.

[69] C. Bierwisch, T. Kraft, H. Riedel, and M. Moseler, "Three-dimensional discrete element models for the granular statics and dynamics of powders in cavity filling," *Journal of the Mechanics and Physics of Solids*, vol. 57, no. 1, pp. 10–31, 2009.

[70] N. J. Brown, J. F. Chen, and J. Y. Ooi, "A bond model for dem simulation of cementitious materials and deformable structures," *Granular Matter*, vol. 16, no. 3, pp. 299–311, 2014.

[71] G. W. Delaney, R. D. Morrison, M. D. Sinnott, S. Cummins, and P. W. Cleary, "Dem modelling of non-spherical particle breakage and flow in an industrial scale cone crusher," *Minerals Engineering*, vol. 74, pp. 112–122, 2015.

[72] S. Luding, K. Manetsberger, and J. Müllers, "A discrete model for long time sintering," *Journal of the Mechanics and Physics of Solids*, vol. 53, no. 2, pp. 455–491, 2005.

[73] C. Martin, B. Bouvarda, and S. Shima, "Study of particle rearrangement during powder compaction by the discrete element method," *Journal of the Mechanics and Physics of Solids*, vol. 51, no. 4, pp. 667–693, 2003.

[74] A. Shafie, J. W. Pro, R. Martini, and F. Barthelat, "The very hard and the very soft: Modeling bio-inspired scaled skins using the discrete element method," *Journal of the Mechanics and Physics of Solids*, vol. In Press, 2020.

[75] Z. Shen, M. Jiang, and C. Thornton, "Dem simulation of bonded granular material. part i: Contact model and application to cemented sand," *Computers and Geotechnics*, vol. 75, pp. 192–209, 2016.

[76] B. Soltanbeigi, A. Podlozhnyuk, S. A. Papanicolopulos, C. Kloss, S. Pirker, and J. Y. Ooi, "Dem study of mechanical characteristics of multi-spherical and superquadric particles at micro and macro scales," *Powder Technology*, vol. 329, pp. 288–303, 2018.

[77] P. Wang, Z. Karatza, and C. Arson, "Dem modelling of sequential fragmentation of zeolite granules under oedometric compression based on xct observations," *Powder Technology*, vol. 347, pp. 66–75, 2019.

[78] W. Zhong, A. Yu, X. Liu, Z. Tong, and H. Zhang, "Dem/cfd-dem modelling of non-spherical particulate systems: Theoretical developments and applications," *Powder Technology*, vol. 302, pp. 108–152, 2016.

[79] J. B. Johnson and M. A. Hopkins, "Identifying microstructural deformation mechanisms in snow using discrete-element modeling," *Journal of Glaciology*, vol. 51, no. 174, pp. 432–442, 2005.

[80] C. Willibald, S. Scheuber, H. Löwe, J. Dual, and M. Schneebeli, "Ice spheres as model snow: Tumbling, sintering, and mechanical tests," *Frontiers in Earth Science*, vol. 7, no. September, pp. 1–13, 2019.

[81] Y. T. Feng, K. Han, and D. R. Owen, "Filling domains with disks: An advancing front approach," *International Journal for Numerical Methods in Engineering*, vol. 56, no. 5, pp. 699–713, 2003.

[82] C. Zhang and X. Zhou, "Evaluation of the packing density of non-spherical particles using discrete element cluster algorithm," *Journal of Information and Computational Science*, vol. 9, no. 16, pp. 4969–4977, 2012.

[83] A. Jagota and G. W. Scherer, "Viscosities and sintering rates of composite packings of spheres," *Journal of the American Ceramic Society*, vol. 78, no. 3, pp. 521–528, 1995.

[84] S. Li, J. S. Marshall, G. Liu, and Q. Yao, "Adhesive particulate flow: The discrete-element method and its application in energy and environmental engineering," *Progress in Energy and Combustion Science*, vol. 37, no. 6, pp. 633–668, 2011.

[85] C. L. Martin and R. K. Bordia, "Influence of adhesion and friction on the geometry of packings of spherical particles," *Physical Review E - Statistical, Nonlinear, and Soft Matter Physics*, vol. 77, no. 3, 2008.

[86] B. Gundlach, S. Kilias, E. Beitz, and J. Blum, "Micrometer-sized ice particles for planetary-science experiments - i. preparation, critical rolling friction force, and specific surface energy," *Icarus*, vol. 214, no. 2, pp. 717–723, 2011.

[87] H. Y. Sohn and C. Moreland, "The effect of particle size distribution on packing packing density," *The Canadian Journal of Chemical Engineeirng*, vol. 46, no. 3, pp. 162–167, 1968.

[88] J. D. Locatelli and V. P. Hobbs, "Fall speeds and masses of solid precipitation particles," *Journal of Geophysical Research*, vol. 79, no. 15, pp. 2185–2197, 1974.

[89] J. Y. Delenne, M. S. El Youssoufi, F. Cherblanc, and J. C. Bénet, "Mechanical behaviour and failure of cohesive granular materials," *International Journal for Numerical and Analytical Methods in Geomechanics*, vol. 28, no. 15, pp. 1577–1594, 2004.

[90] Y. He, T. J. Evans, A. B. Yu, and R. Y. Yang, "A gpu-based dem for modelling large scale powder compaction with wide size distributions," *Powder Technology*, vol. 333, pp. 219–228, 2018.

[91] G. Lian, C. Thornton, and M. J. Adams, "Discrete particle simulation of agglomerate impact coalescence," *Chemical Engineering Science*, vol. 53, no. 19, pp. 3381–3391, 1998.

[92] M. J. Metzger and B. J. Glasser, "Numerical investigation of the breakage of bonded agglomerates during impact," *Powder Technology*, vol. 217, pp. 304–314, 2012.

[93] Y. Ouyang, Q. Yang, and X. Chen, "Bonded-particle model with nonlinear elastic tensile stiffness for rock-like materials," *Applied Sciences (Switzerland)*, vol. 7, 2017.

[94] D. O. Potyondy and P. A. Cundall, "A bonded-particle model for rock," *International Journal of Rock Mechanics and Mining Sciences*, vol. 41, no. 8 SPEC.ISS., pp. 1329–1364, 2004.

[95] M. Kohonen, N. Maeda, and H. Christenson, "Kinetics of capillary condensation in a nanoscale pore," *Physical Review Letters*, vol. 82, no. 23, p. 4667, 1999.

[96] H. Christenson, "Phase behaviour in slits—when tight cracks stay wet," *Colloids and Surfaces A: Physicochemical and Engineering Aspects*, vol. 123, pp. 355–367, 1997.

[97] J. N. Israelachvili, *Intermolecular and surface forces*. Academic press, 2011.

[98] C. D. Willett, M. J. Adams, S. A. Johnson, and J. P. K. Seville, "Capillary bridges between two spherical bodies," *Langmuir*, 2000.

[99] U. Welling and G. Germano, "Efficiency of linked cell algorithms," *Computer Physics Communications*, vol. 182, no. 3, pp. 611–615, 2011.

[100] J. K. Kruschke, *Doing Bayesian Data Analysis*, vol. 81. Academic Press, 2 ed., 2015.

[101] J. S. Marshall, "Discrete-element modeling of particulate aerosol flows," *Journal of Computational Physics*, vol. 228, no. 5, pp. 1541–1561, 2009.

[102] Klaus-Jurgen-Bathe, *Finite Element Procedures*. Prentice Hall, Peareson Education Inc, second ed., 2014.

[103] K.-J. Bathe, *Finite element procedures*. Klaus-Jurgen Bathe, 2006.

[104] R. G. Budynas and J. K. Nisbett, *Shigley's Mechanical Engineering Design*. Mc Graw Hill Education, 10 ed., 2015.

[105] K. Pearson, E. Pearson, and N. Johnson, *Tables of the Incomplete Beta Function*. Cambridge University Press, 2nd ed., 1968.

[106] S.-J. L.Kang, *Sintering -Densification, Grain Growth, and Microstructure*. Burlington, MA: Elsevier Butterworth-Heinemann, 2005.

[107] H. H. Jellinek, "Liquid-like (transition) layer on ice," *Journal of Colloid And Interface Science*, vol. 25, no. 2, pp. 192–205, 1967.

[108] N. Maeda, J. N. Israelachvili, and M. M. Kohonen, "Evaporation and instabilities of microscopic capillary bridges," *Proceedings of the National Academy of Sciences*, vol. 100, no. 3, pp. 803–808, 2003.

[109] M. E. Gurtin, "A gradient theory of single-crystal viscoplasticity that accounts for geometrically necessary dislocations," *Journal of the Mechanics and Physics of Solids*, vol. 50, no. 1, pp. 5–32, 2002.

[110] E. M. Schulson and A. L. Fortt, "Friction of ice on ice," *Journal of Geophysical Research*, vol. 117, no. October, pp. 1–18, 2012.

[111] S. Sukhorukov and S. Løset, "Friction of sea ice on sea ice," *Cold Regions Science and Technology*, vol. 94, pp. 1–12, 2013.

[112] K. M. Salerno, D. S. Bolintineanu, G. S. Grest, J. B. Lechman, S. J. Plimpton, I. Srivastava, and L. E. Silbert, "Effect of shape and friction on the packing and flow of granular materials," vol. 98, pp. 050901–1 to 050901–5, 2018.

[113] L. Arnaud, J. M. Barnola, and P. Duval, "Physical modeling of the densification of snow / firn and ice upper part of polar ice sheets," *Physics of Ice Core Records*, pp. 285–305, 2000.

[114] C. Willibald, H. Löwe, T. Theile, J. Dual, and M. Schneebeli, "Angle of repose experiments with snow : role of grain shape and cohesion," *Journal of Glaciology*, vol. 66, no. 258, pp. 658–666, 2020.

Department of TVM
Division of Experimental mechanics

ISSN 1402-1757
ISBN 978-91-8048-234-9
ISBN 978-91-8048-235-6

Luleå University of Technology 2023

Print: Lenanders Grafiska, 462325

LULEÅ
UNIVERSITY
OF TECHNOLOGY